INSTABILITY OF A HIGH PRESSURE COMPRESSOR EQUIPPED WITH HONEYCOMB SEALS

by

Massimo Camatti

Giuseppe Vannini

Centrifugal Compressor Design Engineer

GE Oil & Gas Nuovo Pignone

Florence, Italy

John W. Fulton

Distinguished Engineering Associate

ExxonMobil Research Engineering

Fairfax, Virginia

and

Fred Hopenwasser

Division Staff Engineer

ExxonMobil Development Company

Houston, Texas

Massimo Camatti is with GE Oil & Gas Nuovo Pignone, in Florence, Italy.

Giuseppe Vannini is a Design Engineer in the Nuovo Pignone Centrifugal Compressor NPI department, GE Oil & Gas, in Florence, Italy. He joined Nuovo Pignone in 2001 and is mainly dedicated to the rotordynamics discipline. Mr. Vannini follows NPI projects focused on the improvement of the knowledge of centrifugal compressor rotordynamics (especially labyrinth and honeycomb seals dynamic effects).

Mr. Vannini received an M.S. degree (Mechanical Engineering, 1999) from Pisa University, and he is currently a part time Ph.D. student (Mechanical Engineering) at the same institution.

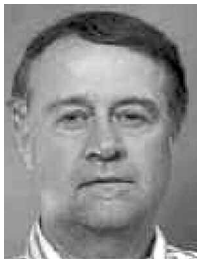

John W. Fulton is a Distinguished Engineering Associate with ExxonMobil Research and Engineering Company at Fairfax, Virginia. In his 31 years with Exxon, he has worked in all phases of machinery engineering and in research and development. Mr. Fulton enjoyed years of assignments in Libya, Venezuela, Alaska, London, and Kuala Lumpur. He has published papers on case histories of vibration problems caused by rotordynamic instability and by rotating stall in high pressure centrifugal compressors. He is coinventor of six U.S. Patents.

Mr. Fulton has a B.S. degree (Mechanical Engineering) from New Jersey Institute of Technology.

ABSTRACT

A two casing (three-stage) high-pressure injection compressor train driven by a gas turbine via a gearbox was full load and full speed performance tested to demonstrate satisfactory aerothermal and rotordynamic performance. During the PTC 10 (1997) Type I testing, rotor instability was observed on the back-to-back (first and second stage) compressor casing. The third stage final compressor casing exhibited anomalous rotor centerline positions in the bearings and rotating stall. This paper discusses the technical analysis, resolution, and retesting to resolve the rotor instability, rotor equilibrium/synchronous response, and rotating stall issues experienced during the testing. It also shows the need for additional joint industry research to better understand and analyze the use of honeycomb seals in hydrocarbon-gas centrifugal compressors.

THE KIZOMBA A PROJECT AND COMPRESSOR TRAIN

The Kizomba A Project high pressure (HP) compressor trains' objectives are to compress associated (hydrocarbon) gas for fuel gas source and reinject as well as compress lift gas for crude oil production. The Kizomba A project is designed to produce 250,000 barrels of oil per day. The associated gas and lift gas will require the two HP compressor trains to handle 144.4 MMscm per day per train. The HP compressor trains will be installed and operate on a floating production storage and off-loading (FPSO) vessel located approximately 100 km (62 miles) offshore Angola. The Kizomba A facilities are operated by Esso Exploration Angola (Block 15) Limited under a production sharing agreement with Sonangol (Angola's national petroleum company). Coventurers in the production sharing agreement are BP Exploration (Angola) Limited, Agip Angola Exploration B.V., and Statoil ASA.

The HP compressor trains are composed of a gas turbine as the driver, a gearbox, and two centrifugal compressor casings with three process stages. The first compressor casing is a back-to-back two-stage compressor (HP first and second stage) with four impellers for each stage. The HP third stage final compressor casing is a straight-through compressor with five impellers. The train layout is shown in Figure 1. The main compressor design features are summarized in Table 1.

The compressors are equipped with the traditional five tilting pads radial bearing with load-on-pads built by Nuovo Pignone. The main bearing geometrical features are summarized in Table 2. The compressor internal seal original design is shown in Table 3. Use Figure 2 and 3 for seal locations on the cross sectional drawing.

The impeller eye seals were tilted teeth labyrinth design to reduce gas leakage, thus providing improved compressor efficiency for both compressor casings. Each tooth of the eye seals is on a smaller diameter than the tooth upstream of it ("stepped"). The balance piston seal on the second stage end for the back-to-back compressor (2BCL 458/A) used teeth-on-rotor type,

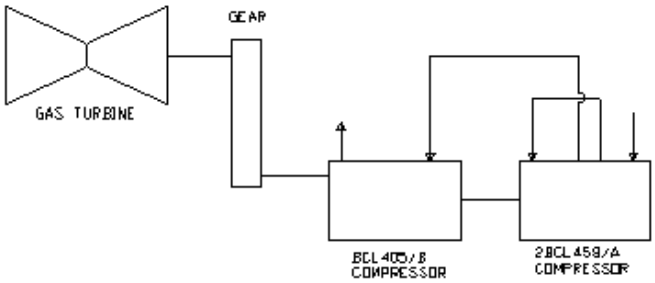

Figure 1. Train Sketch.

Table 1. Main Compressor Design Features.

Compressor Stage	HP 1st Stage	HP 2nd Stage	HP 3rd Stage
Compressor Model	2BCL 458A		BCL 405B
Number of Impellers	4	4	5
Suction Pressure (Bara)	15	46	140
Suction Temperature (?C)	62	38	38
Flow (MM scm/d)	3.88	2.94	2.94
Discharge Pressure (Bara)	48	141	298
Discharge Temperature (?C)	155	139	102
Molecular Weight	21.4	21.4	21.4
Power (kW) w/ Comp Losses	8400	7360	4275
Minimum Hub Diameter (mm)	205		144
Bearing Span (mm)	1983		1517

Table 2. Main Bearing Geometrical Features.

Compressor Casing	Diameter (mm)	Assembly Diametric Clearance (mm)	Preload	L/D	Offset
2BCL 458A	120	0.14	0.6	0.44	60%
BCL 405B	120	0.14	0.6	0.44	60%

Table 3. Compressor Internal Seal Original Design.

Seal Location	Impeller Eye Seals (a)	Interstage Balance Piston (b)	Final Balance Piston (c)
2BCL 458A	Tilted Teeth Labyrinth Seals (Teeth on Stator)	Cylindrical Honeycomb Seal Note 1	Abradable Seal (Teeth on Rotor)
BCL 405B	Tilted Teeth Labyrinth Seals (Teeth on Stator)	NA	Cylindrical Honeycomb Seal (No Shunt)

Note 1: Plugged shunt holes on the interstage diaphragm

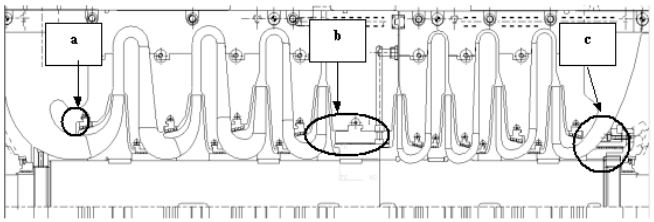

Figure 2. Back-to-Back Compressor Casing Cross Sectional Drawing: Detail of Rotor and Seals (a: Impeller Shroud Seal, b: Honeycomb Interstage Seal, c: Abradable (Final Balance) Seal).

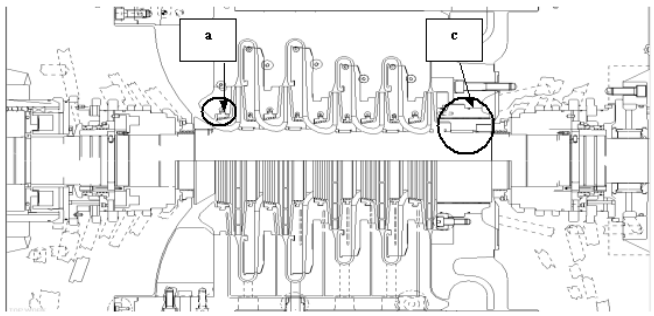

Figure 3. BCL 405B Straight-Through Compressor Casing Cross Sectional Drawing: Detail of Rotor and Seals (a: Impeller Shroud Seal, c: Honeycomb (Final Balance) Seal).

abradable stationary component, and very tight clearance that was selected for improved efficiency. The interstage (center wall) balance piston seal for the 2BCL 458/A casing used a honeycomb (stator side) seal running against a smooth (drum) rotor.

The manufacturer's standard rule for compressors at the pressure level of the 2BCL 458/A is to install a labyrinth seal, but a honeycomb was included in the original design due to concerns about rotor stability. Drillings to supply shunt holes are provided in the original design, but were plugged for the first two test builds. ("Shunt" holes are defined as a feature to bring gas from the discharge volute or diffuser to the entrance of a honeycomb seal or labyrinth seal. The intent is to prevent entry of swirling flow from the back of the impeller into the seal. Because of the diffuser's gain in static pressure, the shunt causes the flow behind the last impeller to go from the seal to the larger radius of the impeller tip, reversing the direction it would go without the shunt.) The shunt passages can be seen in Figure 2 connecting the eighth diffuser with the honeycomb inflow side.

The option of opening the shunts before the start of testing was discussed, but it was decided that shunt holes should not be required based on the manufacturer's original design analysis. At that time, the sensitivity of the honeycomb to the taper of the clearance, to the magnitude of the clearance, and to inlet swirl was not fully appreciated. Opening the shunts causes a small increase in balance piston leakage due to shortening the length available for the seal. On the 2BCL 458/A the change in the rotor's axial thrust is negligible.

The HP third stage, a straight-through compressor casing (BCL 405/B), used a final balance piston seal with a cylindrical honeycomb without a shunt. By "cylindrical" the authors mean that the clearance along the length of the seal is intended to be constant. The impeller eye seals are the same as discussed above.

Both compressor casings are equipped with tandem dry gas seals. The train is coupled between the drive gearbox and the compressor casing using flexible (diaphragm type) couplings.

2BCL 458/A FIRST AND SECOND STAGE COMPRESSOR

Rotordynamic Design

The original rotordynamic design of the compressor was fully compliant with the API 617 Sixth Edition standard. (The compressor was designed in the first half of 2002, before the release of the API 617, 2002, Seventh Edition.). The manufacturer's stability analysis had been performed by taking into account the aerodynamic cross-coupled stiffness (evaluated by the Wachel formula, refer to Equation 1.2-7 in API 617, 2002, Seventh Edition) with the addition of the honeycomb seal coefficients. The dynamic coefficients of the honeycomb seal were evaluated by means of the code described in Kleynhans and Childs (1997). The stability calculations were performed by means of the manufacturer's code based on the Lund approach. These calculations, which were performed with different combinations of bearing clearances and lube oil temperatures, always yielded a positive logarithmic decrement (log dec) without showing any clear sign of potential instability. The stability margin analysis showed a Q_A/Q_0 value of about 0.55 (refer to Figure 1.2-4 in API 617, 2002, Seventh Edition). With only the Wachel effect applied, the log dec is negative; however, the damping coming from the honeycomb was expected to be large enough to stabilize the system.

The stability diagram (Figure 4) showed that the 2BCL 458/A (shown as a solid round dot) was within the manufacturer's experience range. This diagram is similar to the Fulton diagram (Fulton, 1984a, 1984b) but uses criteria based on the manufacturer's experience. On this diagram, the 2BCL 458/A is in an area where the lead author's company requires a more detailed analysis in order to evaluate the seal effects. The diagram shows two lines based on the manufacturer's experience: the continuous line stands for the boundary of the experience while the dashed line is the threshold line beyond which a more detailed stability analysis is required,

according to the internal standard. The API 617 (2002) Seventh Edition similarly separates its stability analysis into levels 1 and 2, in its Figure 1.2-5. For reference, the API line is plotted here (Figure 4) as a dash-dotted line. The 2BCL 458/A is significantly above this line.

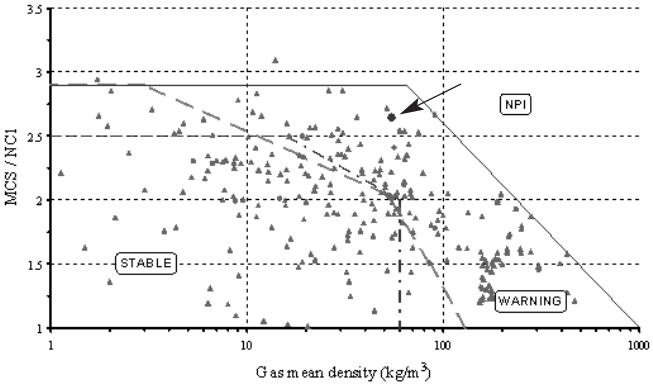

Figure 4. Stability Diagram. (Courtesy GE Oil & Gas)

Initial Load Test Results

The compressor with the original seal configuration showed a subsynchronous frequency suddenly rising when the compressor approached the middle of its operating curve. The subsynchronous frequency at the beginning of the test was as low as 41 Hz and increased with additional running to about 46 Hz (Figure 5). At the 41 Hz point, the gas density at the inflow side of the honeycomb was 44 kg/m^3, at a pressure of 123 bara (1780 psia), and the pressure difference across the honeycomb was 75 bar (1088 psi).

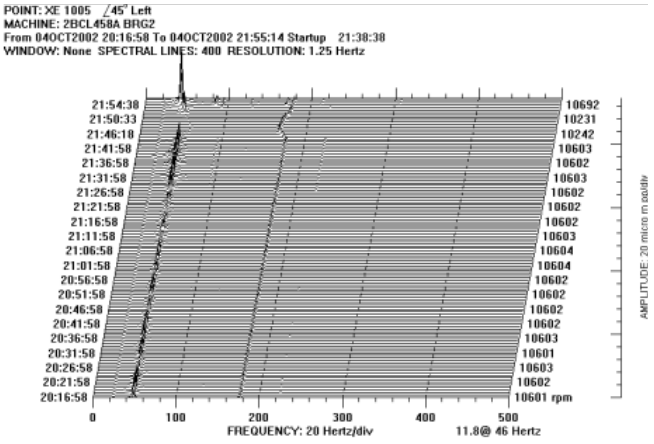

Figure 5. Waterfall Spectrum of Vibrations at Compressor Constant Speed (100 Percent) Showing 46 Hz Subsynchronous Frequency.

Figure 6 shows the second stage head versus flow operating curve with the dot showing the threshold of instability. Here the differential pressure across the interstage seal reached about 80 bar (1160 psi) while at the guaranteed point it should have been 93 bar (1149 psi).

The subsynchronous frequency was very low in comparison to the expected. The first natural frequency for the rotorbearing system was 65 Hz according to calculations. This is confirmed in Figure 7 where the runup on test at low density showed 3800 to 4000 rpm for the peak amplitude speed and phase shift.

During the test it became evident that the subsynchronous frequency was due to a rotordynamic instability, since the frequency was constant with the rotational speed and the amplitude strongly depended on the pressure drop across the interstage seal (i.e., the difference between the first and the second stage discharge pressure).

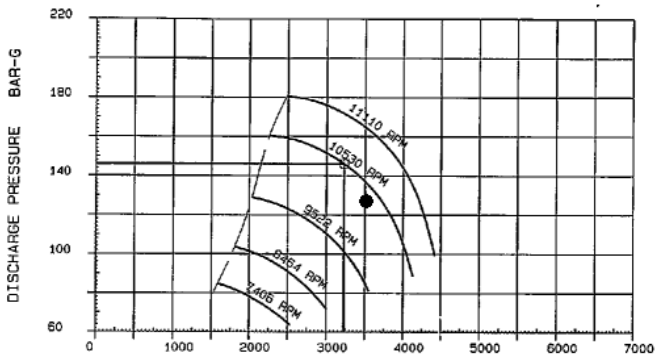

Figure 6. Head Versus Flow for Stage 2 with Onset Point of Instability.

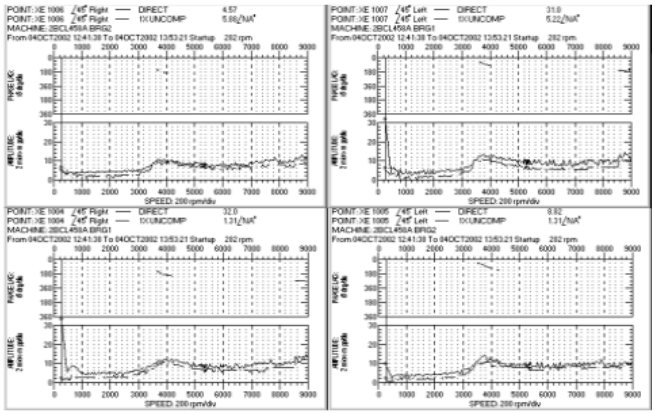

Figure 7. Bodé Plot During Startup Showing Rotor First Critical Speed Near 65 Hz.

During the test a slight contact between the rotor and the stator took place (the cause probably was a sudden operation with one of the control valves in the gas loop system), and the consequence was the shift of the subsynchronous frequency to about 51 Hz (Figure 8). Although the maximum allowable differential pressure was increased somewhat after the increase in frequency, the instability remained. After disassembly of the compressor bundle, signs of contact were found on both the interstage honeycomb seal (Figure 9) and on the balancing piston. The frequency shift phenomenon was explained later by the rotordynamic analysis, which also suggested the final modification to the interstage seal.

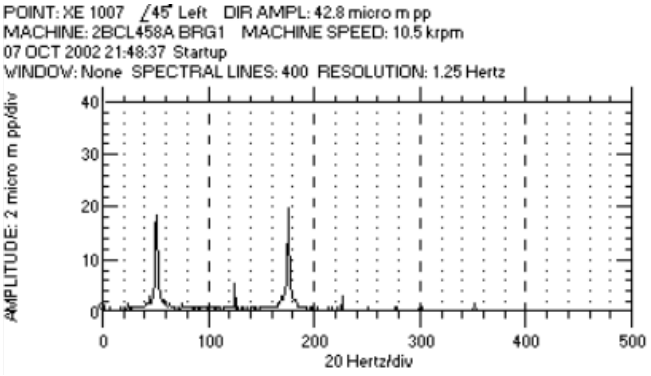

Figure 8. Spectrum of Vibrations at Compressor Constant Speed (100 Percent) Showing 51 Hz Subsynchronous Frequency.

A damped natural frequency code (Murphy, 1993) was used to estimate the net direct and cross-coupled stiffness acting on the

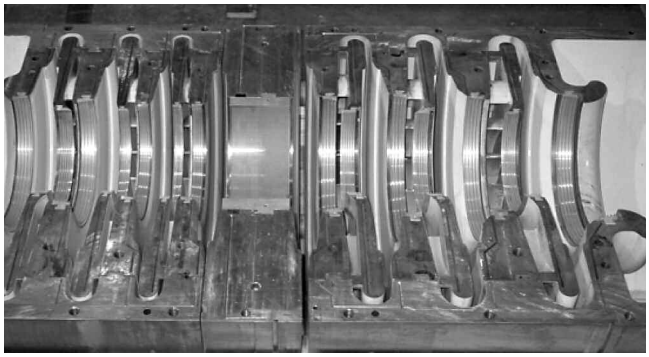

Figure 9. 2BCL 458/A Bundle Half Showing Rub on Inlet Side of Honeycomb Center Seal.

center of the rotor at the threshold of stability. Using bearing coefficients for nominal clearance and oil temperature, the direct stiffness and cross-coupled stiffness inputs were varied until the damped natural frequency matched the value observed on test, while iterating to reach a logarithmic decrement equal to zero. The only forces acting on the rotor in this calculation were the bearings and the direct and cross stiffness just mentioned. At 10,535 rpm, to reach the stability threshold at 52 Hz requires a direct stiffness of negative 160,000 lbf/in (−28 kN/mm) and a cross stiffness of 27,000 lbf/in (4.7 kN/mm). Because the impeller eye labyrinths are not expected to produce much direct stiffness, this large negative direct stiffness is attributed to the honeycomb. Also, the assumption of the design analysis given above, that the honeycomb would offset any destabilizing forces from the eye labyrinths, did not seem to hold.

The design analysis discussed above mentioned the Wachel number. Accordingly, the Wachel number is given here for reference, without any consideration of the theoretical basis of the Wachel number. Calculated according to the API 617 (2002) Seventh Edition, it equals 5.7 kN/mm (33,000 lbf/in) at the rated point. This is similar to the threshold aerodynamic cross coupling calculated above for conditions, which were somewhat below rated.

Honeycomb Seal Behavior

The main cause for the instability seemed to be the honeycomb seal. The dynamic coefficients, calculated with a computer software program, showed that K_{eff} decreased with decreasing whirling frequency down to a negative value in the frequency range of interest (Figure 10) for the taper diverging in the direction of leakage flow. In Figure 10, a taper of 0.12 mm (.005 inch, radial) would be required to explain the first natural frequency depression to 41 Hz.

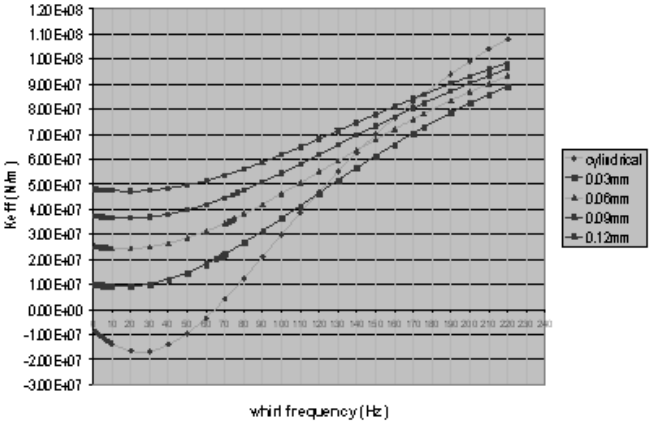

Figure 10. Effect of Tapering on Honeycomb Effective Stiffness.

This software calculation showed that varying the inlet and outlet radii should control stiffness. By reducing the outlet radius (giving the honeycomb a convergent conical shape in the direction of leakage flow), the negative direct stiffness values were shifted toward the low frequency region and then disappeared. Also the test outcomes seemed to confirm this trend. Because the visual inspection of the honeycomb showed signs of rubbing on the inlet side of the seal, it is evident that it was made slightly convergent by the contact with the rotor. Referring to Figure 10 shows that in the 40 to 50 Hz range, the direct stiffness increases with larger inlet clearance, which will raise the subsynchronous frequency.

A sensitivity analysis was performed to see the effect of the tapering (defined as the difference between the inlet and outlet radius) on the natural frequency and logarithmic decrement (Figure 11 and 12). Comparing these figures shows that an increase in the convergence of the taper increases the natural frequency while decreasing the log dec. To get a larger log dec (to be stable), the authors considered using a diverging taper. However, because they had not been able to predict the instability, they were concerned that there was some inaccuracy in their modeling.

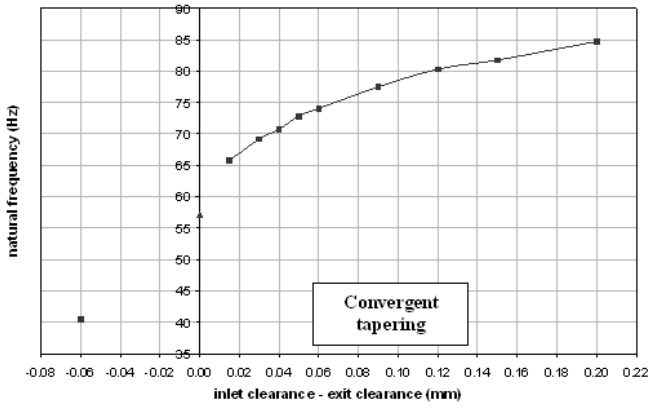

Figure 11. Effect of Tapering on Rotor First Natural Frequency.

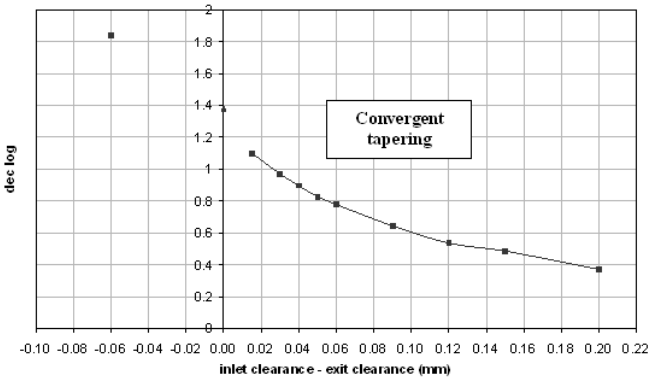

Figure 12. Effect of Tapering on Rotor Logarithmic Decrement.

Note that the damped natural frequency calculation finds the log dec and the natural frequency (here forward whirl of the first bending frequency) using inputs of the frequency independent effective stiffness and effective damping for the honeycomb. However, for a honeycomb the effective stiffness and effective damping is frequency dependent, therefore one must iterate to close on frequency. Thus, the damped natural frequency calculation is entangled with the honeycomb characteristics. Figure 13 shows that the effective damping can become highly negative (very destabilizing) as the whirling frequency drops below 40 Hz (without shunt.). Because the authors felt that the software calculation correctly predicted the trends with frequency, but may be somewhat inaccurate regarding the exact frequency, they felt it safer to avoid diverging taper and depressed natural frequencies.

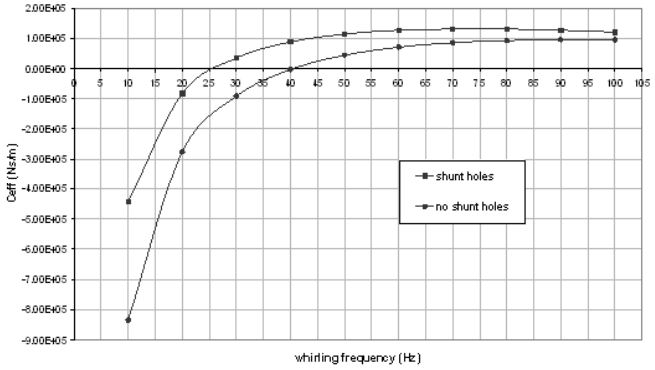

Figure 13. Effect of Shunt Holes on Honeycomb Damping.

Retrospectively playing with the calculation, the authors have calculated that large diverging clearances may lead to very low natural frequencies and very negative log decs.

As a first remedy, it was decided to have 0.06 mm (.002 inch) as radial convergent tapering in order to have the best trade-off between the need of increasing the frequency as much as possible and the need of a sufficient damping.

Honeycomb Finite Element Method Analysis

To guarantee the selected tapering, a finite element method (FEM) analysis of the seal plus the balancing piston was performed. In fact the clearance in working conditions can be strongly affected by the centrifugal force on the balancing piston that causes a gap reduction and by the temperature or pressure effects that produce not negligible deformations of the seals. The meridian section of the two elements was studied (Figure 14 and Figure 15). For the 2BCL 458/A honeycomb seal, which is cut in half at the bundle part line, the axisymetric FEM is an approximation to ease the analysis.

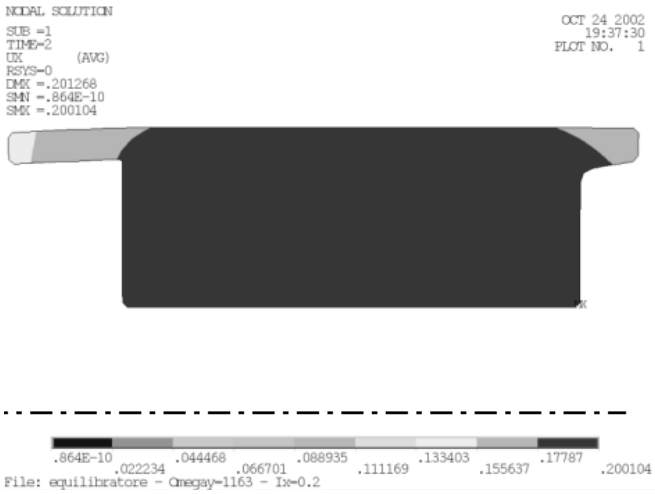

Figure 14. FEM Results (Radial Displacements) for Balancing Piston.

The finite element analysis (FEA) results confirmed that the working seal clearance was divergent. To produce the new design objective of 0.06 mm (.002 inch) as radial convergent tapering clearance at rated conditions, the cold clearance of the honeycomb was bored to a convergent taper of 0.12 mm (.005 inch) on a side (radial) based on the FEA.

Concerning the lack of damping, it was decided to open the shunt holes in order to decrease the gas swirl at the seal entrance. This action could enhance the damping of the seal without disturbing its stiffness properties obtained through the conical shape. Figure 13 shows that the C_{eff} of the shunted honeycomb is about two times greater in the region of interest near 60 Hz.

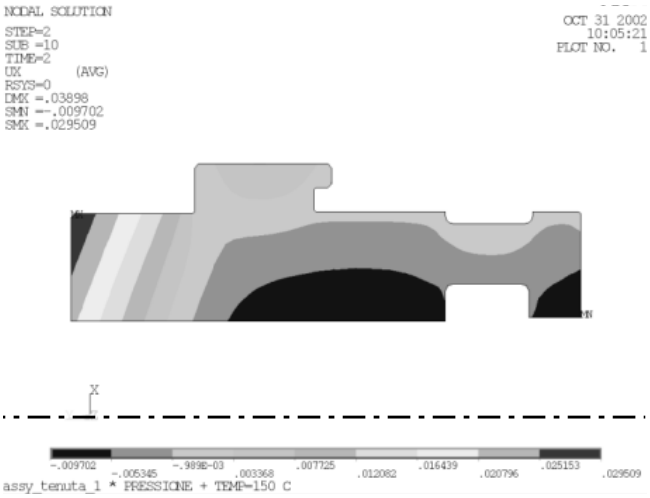

Figure 15. FEM Results (Radial Displacements) for Honeycomb Seal.

Alternate Seal Options

The effects of all the other seals in the system were computed and imposed on the rotor in addition to the honeycomb in order to consider the options for the correction. The tooth-on-rotor seal at the second stage suction was included. Moreover the possibility to install a shunted labyrinth seal on the interstage balancing piston was investigated since the honeycomb application seemed to be quite critical and very sensitive to the operating clearance. The impeller shroud's short labyrinth seal coefficients were evaluated through a suite of software codes developed by a major university. These seals did not have swirl brakes.

Considering the option of using a labyrinth instead of a honeycomb for the center seal, Figure 16 shows that a labyrinth with shunt would give slightly negative log decrements, while a cylindrical honeycomb, with shunt, should be very stable. Therefore, replacing the honeycomb with a labyrinth was not a viable option.

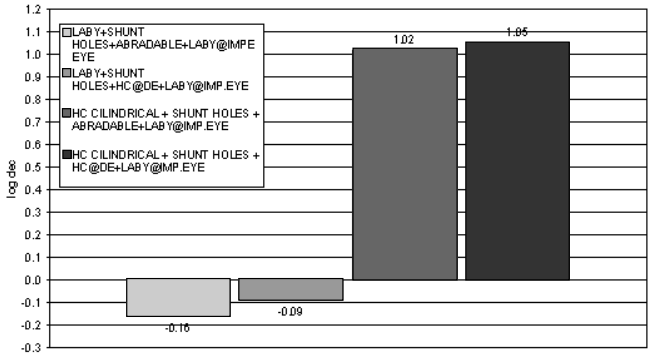

Figure 16. Options for Seal Configurations.

The results of the above calculations also showed that the traditional eye labyrinths could slightly decrease the log decrement. Therefore a special type of short slotted seal (shown as "webbed seal" in Figure 17) was chosen for the eyes. The web seals' effect on the rotordynamic stability is mainly based on the manufacturer's experience. At the present time no available code can properly model their dynamic behavior. [Only a computational fluid dynamics (CFD) approach analysis could be utilized to try to evaluate their effect, but CFD would have been time consuming and unsuitable for such a pressing case]. So the modifications decided for the following test were the webbed seals on the impeller shrouds and a honeycomb with shunts for the center seal.

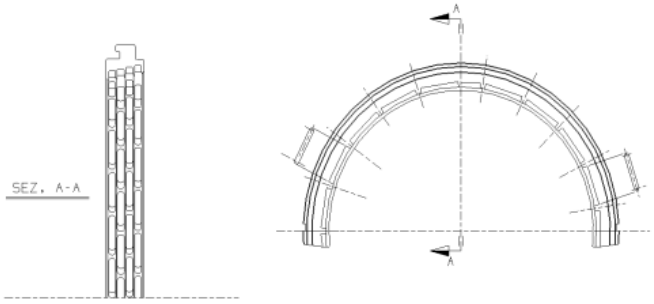

Figure 17. Webbed Seal Installed on Impeller Shrouds in Final Configuration.

Test Results for HP1 and HP2
Body—Without and with Shunts

A second test was performed first with the newly designed set of seals installed and the shunt holes plugged. Thus the effect of the shunt on the honeycomb would be made clear. Without the shunt, the subsynchronous frequency was still present, but now it was around the expected value of 65 Hz, about 25 percent more than in the previous test (Figure 18.) The maximum allowable differential pressure increased slightly reaching about 90 bar (1305 psi). The instability was not yet cured but the theoretical predictions regarding the recovery of the honeycomb stiffness were confirmed by the experimental results.

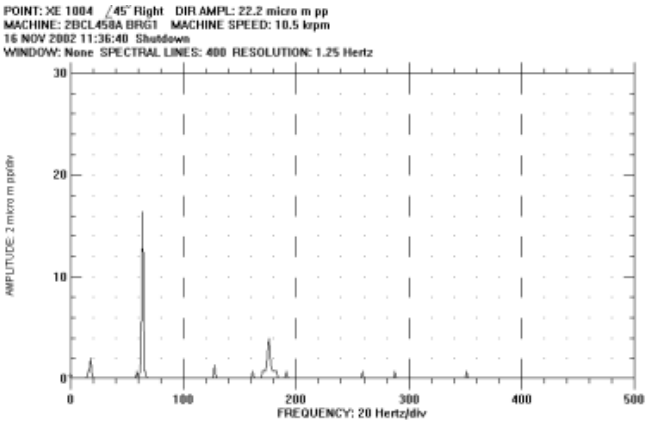

Figure 18. Spectrum of Vibrations Showing Recovered 65 Hz Subsynchronous Frequency.

Again a damped natural frequency code was used to estimate the net direct and cross stiffness acting on the center of the rotor at the threshold of stability. Using bearing coefficients for nominal clearance and oil temperature, the direct stiffness and cross-coupled stiffness inputs were varied until the damped natural frequency matched the value observed on test, while iterating to reach a logarithmic decrement equal to zero. At 10,535 rpm, to reach the stability threshold at 65 Hz requires a direct stiffness of positive 30,000 lbf/in (5.2 kN/mm) and a cross stiffness of 45,000 lbf/in (7.9 kN/mm) acting on the center of the rotor. These coefficients reflect the combined effects of the honeycomb (without shunt) plus the eye labyrinths acting on the first forward bending mode. At this point the pressure upstream of the honeycomb was 141 bara (2045.03 psia) and the differential pressure across it was 87 bar (1262 psi).

The compressor was disassembled and the plugs were removed from the shunts. Figure 19 is a photograph of the honeycomb after running at the threshold of stability, before the shunts were opened. The web seal can also be seen. The honeycomb shows rub marks on the inlet side of the seal. These marks covered the entire circumference. These rub marks raise the question of whether the clearance was diverging, which was not expected from the FEM analysis. Because the honeycomb is near the center of the rotor, this rub is not likely to be due to a conical shape of the rotor first bending mode.

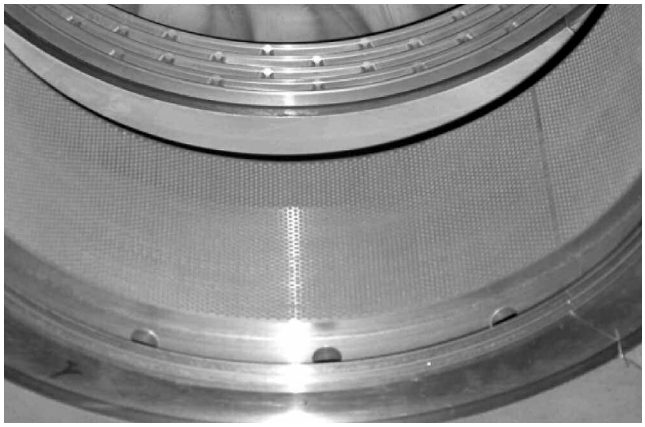

Figure 19. Honeycomb with Provisions for Shunt (Closed) after Running with Instability.

With the shunts finally open the compressor ran without any subsynchronous frequency through all its operating range, reaching not only the 100 bar (1450 psi) differential pressure condition but also the surge flow (about 120 bar, 1740 psi) condition. Now the problem was definitively fixed (refer to Figure 20 for the final vibration spectrum of the rotor).

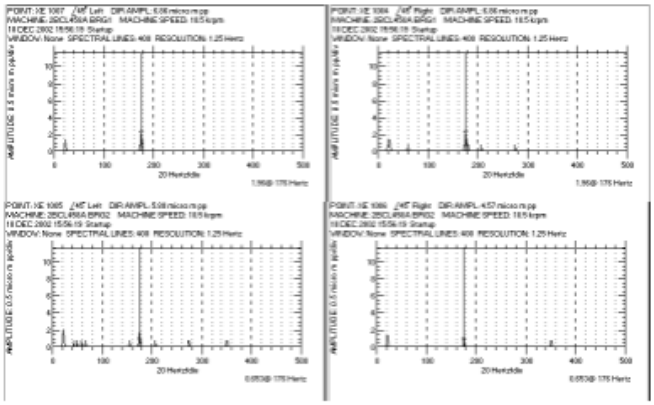

Figure 20. Spectrum of Vibrations Showing Absence of Instability at 65 Hz Frequency.

The authors' interpretation of the instability problem depends on recognizing the following rotordynamic behavior:

- Negative effective damping (shown in Figure 15 for the honeycomb) causes instability.
- Negative effective stiffness (shown in Figure 10 for the honeycomb) reduces the first bending frequency of the rotor.
- Negative effective stiffness does not directly cause rotor instability, but by reducing the first bending frequency it reduces the ability of the rotor to resist destabilizing forces. As discussed above, an effective direct stiffness of −160,000 lbf/in caused the rotor to reach the threshold of instabilty with effective cross stiffness of 27,000 lbf/in. Raising the effective direct stiffness to +30,000 lbf/in raises the resistance of the rotor to an effective cross stiffness of 45,000 lbf/in.
- Below 60 Hz, this honeycomb produces negative effective stiffness (Figure 10) if it is not tapered with converging clearance. And most important, its effective damping becomes increasingly and strongly negative with decreasing whirl frequency.

The authors' interpretation of the instability problem is as follows:

- The shunt was required to eliminate the instability. It stopped the entry of swirling gas into the honeycomb, thus increasing the effective damping as shown in Figure 13.
- Convergent tapering of the honeycomb eliminated the negative effective stiffness, and thus eliminated the depression of the first bending frequency and its interaction with the honeycomb damping. However, convergent taper was not sufficient to eliminate the instability.

BCL 405/B THIRD STAGE COMPRESSOR

The initial test of the third stage compressor showed vibration higher than the job specified limit of 37 microns peak-to-peak direct. The maximum observed was 54 microns on the discharge end while running at 10,536 rpm. Two causes were found, one attributed to rotating stall and the other to an erratic synchronous response associated with the honeycomb's rotordynamic impedance and anomalous bearing centerline positions. The stall will be discussed first.

Rotating Stall

This compressor has vaneless diffusers on all five stages. The diffusers are pinched to avoid rotating stall in the operating range. (Pinch is defined as the width of the diffuser parallel section, b4 divided by the impeller tip passage width, b2.) The pinch ratios, from the first wheel to the last are shown in Table 4. The inlet profile of the diffuser follows the manufacturer's proprietary elliptical profile, designed to give stall performance similar to Nishida and Kobayashi's (Kobayashi, et al., 1990) rapid pinch, but with less efficiency degradation.

Table 4. HP3 Diffusers—Pinch Ratios.

Stage:	1	2	3	4	5
b4/b2	0.52	0.53	0.5	0.5	0.3

Design review by the owners suggested that rotating stall may occur near the operating range, with the earliest stage to stall being the first diffuser at about 77 percent flow. The predicted stalls are shown on the compressor map of Figure 21, which shows stall occurring at the inception lines, labeled by stage. This prediction contains a four degree margin above Nishida and Kobayashi's (Kobayashi, et al., 1990) criteria, to allow for not meeting their rapid pinch schedule. Refer to Fulton and Blair (1995) for discussion of this margin.

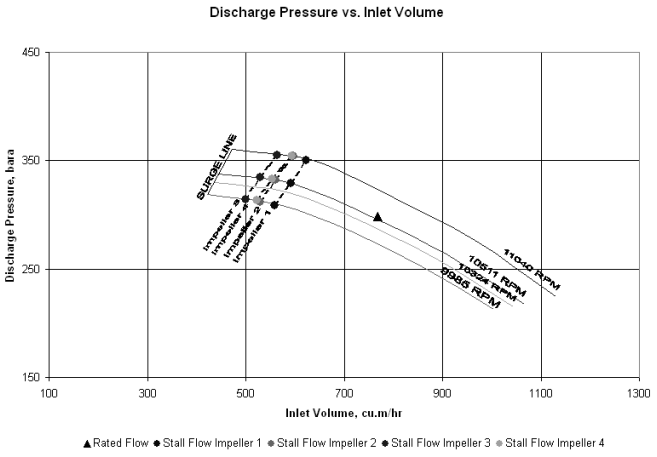

Figure 21. Discharge Pressure Versus Inlet Volume.

The last stage diffuser could be expected to produce the largest vibration if it stalled. As a measure against this risk, the manufacturer applied more pinch to remove the predicted stall inception from the operating range. The expected stall of the last stage is not shown on Figure 21, as it is far to the right.

To address any stalls that may occur, the manufacturer provided replaceable diffuser walls to enable width adjustment by changing parts in the aero bundle. For the load test, pressure transducers were connected to each return bend to measure both the static pressure and the pulsation from any stall that might occur. The stages that are stalling can be identified from the relative magnitude of the pulsation signals.

During the load test, rotating stall could be seen in the vibration spectrum, Figure 22, which is for the probe at the discharge end bearing. The largest component has a frequency of 12.4 Hz or 7.1 percent of running speed. The stall frequency can also be seen in sidebands on the running speed vibration.

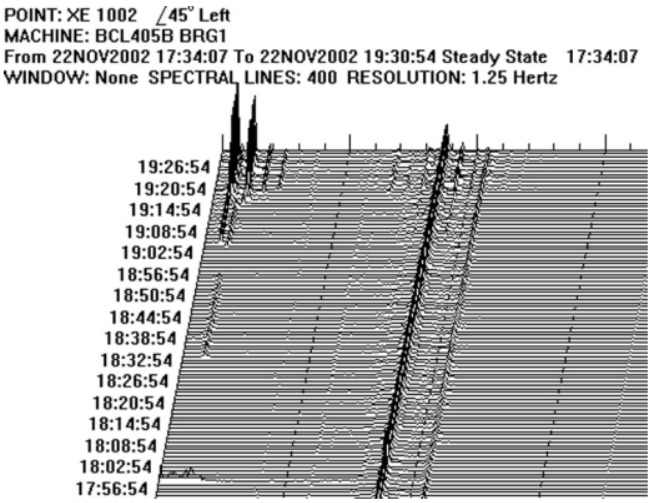

Figure 22. HP3 Performance Map Showing Predicted Stall Inception.

During this testing seven data points were taken at rated speed with decreasing flow. These points can be expressed as a fraction of rated volume flow. The API 617 (2002) limit on vibration component amplitude below running speed is 20 percent of the overall allowable. The vibration components at stall frequency can be expressed for each point as a fraction of allowable. The two sets of numbers can be compared in Table 5 (the two vibration values shown as 0.00 are missing data, not actually zero). As can be seen, the last two points exceed the allowable. These points do not form a smooth line, but one can say excessive stall induced vibrations were present at 67 percent flow. This is lower than the prediction of 77 percent for the first stall, showing the four degree margin mentioned above is too conservative in the elliptical pinch schedule.

Table 5. HP3 Stall Inception Points.

Data Point:	1	2	3	4	5	6	7
Volume Flow / Rated	0.81	0.80	0.77	0.77	0.75	0.67	0.66
Sub-synchronous Vibration/Allowable	0.68	0.00	0.00	0.58	0.27	1.51	4.05

The criteria for rotating stall by Nishida and Kobayashi is detailed by Fulton and Blair (1995). The essence of the criteria is to compare the mean angle of the gas entering the parallel wall section of the diffuser with the critical angle where stall occurs. The critical angle depends on the geometric proportions of the impeller and diffuser and the shape of the diffuser inlet. Their criteria for stall inception, calculated for the BCL 405/B, are shown in Table 6.

Table 6. HP3 Nishida-Kobayashi Criteria Angles.

Stage:	1	2	3	4	5
Alpha4criteria (degrees)	12.3	12.2	12.4	12.4	14.1

It is interesting to compare the predicted inception angles to those found during the full load test. To do so requires calculating the mean gas angle from the test data, using the dimensions of the impellers and diffusers. A right triangle with the tangential gas velocity (as horizontal) and the radial gas velocity (as vertical) defines the mean gas velocity. For this test, the tangential gas velocity was calculated from the work input to each impeller. The radial gas velocity was calculated from the mass flow and the density of the gas at the impeller tip. The trick, as explained in Fulton and Blair (1995), is to use the pressure measured at each return bend to apportion the head and gas density to each impeller, given the flange-to-flange performance test data. For this calculation, efficiency was distributed over the stages based on the flange-to-flange efficiency measured on test.

Figure 23 shows the comparison. The horizontal axis is the difference between the predicted inception angle for each diffuser and the actual gas angle calculated for each test point. The vertical axis is the pulsation found at each return bend. It is shown in volts measured with a transducer and charge amplifer. The vertical line at zero degrees reaching to 0.5 V gives a visual indication of the comparison. Stall is predicted to occur to the left of this line. Pulsation voltage above this line was found to correlate with excessive rotor vibration as defined by "Allowable Vibration" in Table 5. There is one outlier at 0.5 V and 1.0 degree for stage 1. With the exception of the outlier, it can be seen the pulsation is small to the right of the line, but grows to the left. Stage 1 has the largest values on the left. (Stage 5 is well clear of stall, off the plot to the right, and was not plotted for clarity.)

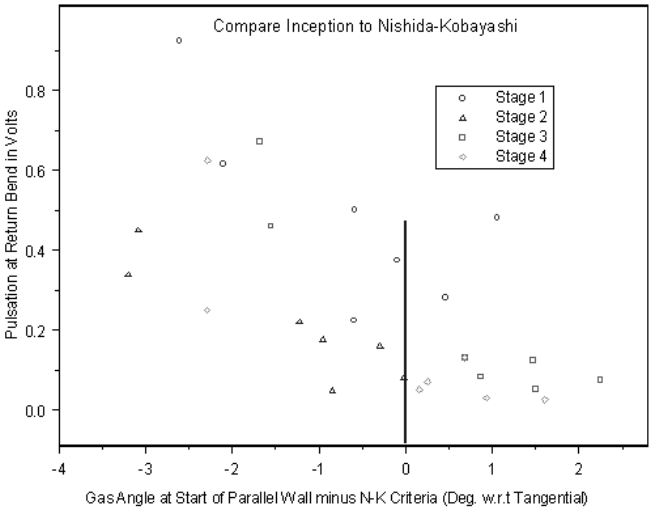

Figure 23. Validation of Nishida-Kobayashi Criteria for Rotating Stall.

To move the rotating stall inception points to the left on the performance map (Figure 21), thus putting them out of the operating range of the compressor, the removable diffuser plates were changed to the pinch values shown in Table 7.

Table 7. HP3—Revised Pinch Schedule.

Stage:	1	2	3	4	5
b4/b2 (modified)	0.3	0.4	0.4	0.4	0.3

Upon reassembly and retest the BCL405/B ran at the maximum continuous speed of 11,132 rpm and behind the surge control line at an inlet volume of 551 m^3/h. Rotating stall appeared only after passing behind the intended surge control line, therefore it will not be seen in operation. At that point, the maximum subsynchronous vibration was 22 microns at 17 Hz (9.2 percent of rpm) on a discharge end probe. The other three probes showed less vibration at the same frequency.

Synchronous Response and Bearing Centerline Position

Early in the full load test for this body, when the pressure in the test loop was increased, the synchronous vibration increased at the same time. The phase angle was unaffected (Figure 24). At times, the combination of the synchronous response and the rotating stall exceeded the allowable vibration of 37 microns, direct.

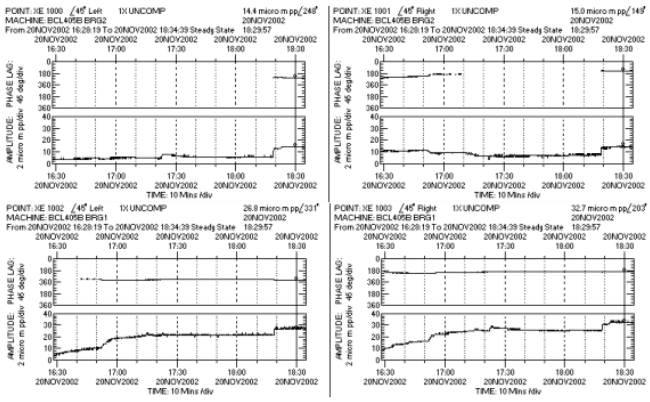

Figure 24. Trend of Synchronous Vibration at Constant Speed and Increasing Pressure. Top Two Trends are for Discharge End Bearings, and Bottom Two are for Suction.

Repeating the testing to reexamine the problem showed a general trend over time toward somewhat reduced vibration. The shaft centerline position, known from the gap voltage, was unusual, but not repeatable. In one case, Figure 25 (shown on the left side) the shaft rose about 140 microns on the discharge of the casing, during startup and loading. The 140 microns is the full diametral clearance of the tilt pad bearing. Therefore the journal was running in the top of the bearing, instead of on the bottom, as would be expected if the rotor weight provided the only major load on the bearing. At the same time the other bearing (right side plot) showed similar behavior, except that it fell back to an intermediate position above the bearing center.

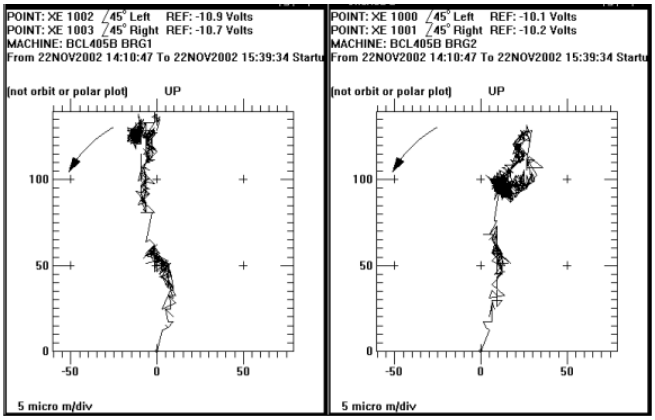

Figure 25. Shaft Centerline Position in Bearings, from Zero Speed to Full Speed and Intermediate Pressure. Left Figure is for Discharge End Bearing and Right is for Suction. At Full Speed PdDp Ranged from 12,000 to 23,000 Bar^2.

The centerline position also varied with pressure. PdDp can be defined as the product of discharge pressure (the pressure entering the honeycomb) times the pressure difference across the second section of the compressor (and across the honeycomb.). For Figure 26 the PdDp varied significantly from Figure 25. However the centerline did not raise monotonically with PdDp as might be expected, but was higher for intermediate values of PdDp as shown in Figure 25. This tends to discount the remote possibility that the centerline was affected by the diaphragm coupling torque, because torque increased with PdDp.

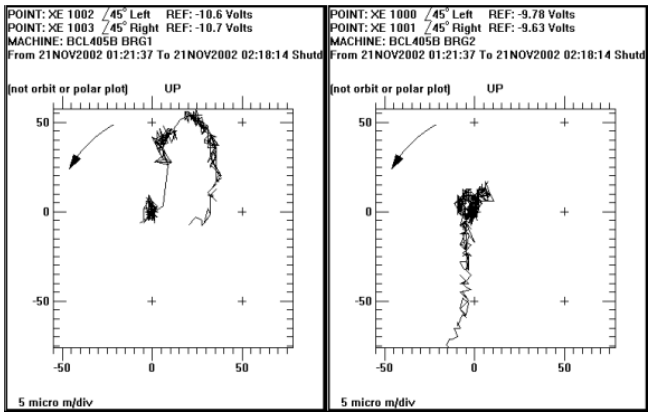

Figure 26. Shaft Centerline Position in Bearings, from Full Speed and High Pressure to Zero Speed. Left Figure is for Discharge End Bearing and Right is for Suction. At Full Speed PdDp Ranged from 55,000 to 70,000 Bar².

Based on the experience with the 2BCL 458 honeycomb, which showed strong negative stiffness, a reasonable hypothesis is that the rotor was lifted to the top of the bearing by the honeycomb. Attempts to calculate the effect of bearing load on the synchronous response were not satisfactory. Nevertheless, it was decided to perform an FEM analysis to determine the distortion of the honeycomb bore. It was found that the cold clearance needed 75 microns taper per side to compensate for distortion, so that the clearance would be uniform along the length of the honeycomb, at rated conditions.

On disassembly, a coating on the balance piston was found rubbed, showing the operating clearance had been divergent along the length of the honeycomb in the direction of the flow and confirming the FEM analysis. The rubbing also explained the improved behavior at the test proceeded, much the same as found for the 2BCL 458/A, where the divergent taper was partially rubbed away. The taper bore honeycomb was installed. No shunt was used. On retest, the unusual centerline positions became more normal. The synchronous response was satisfactory, meeting the 37 microns, direct, at all points in the operating flow and speed range of the compressor.

After the test a calculation of the static bearing loads was made over a broad range of direct and cross-coupled stiffness (at zero whirl frequency, as the coefficients can be frequency dependent). The rotor was treated as a rigid body with the stiffness applied at the two bearings and at the honeycomb seal. Four simultaneous equations are required to solve for equilibrium in response to the rotor weight. Because the bearing loads can be high, a nonlinear bearing model was used to ensure reasonable journal displacements.

This nonlinear bearing model was made by calculating the eccentricity of the bearing at various loads (100 to 5000 lbf) using a solver by Nicholas (1979). The resulting plot of load versus eccentricity fit a straight line well on log-log coordinates. The resulting model is shown in Figure 27 over the full range needed to calculate the static rotor equilibrium.

Figures 28 and 29 show the resulting bearing loads as a fraction of rotor weight. (At zero direct and zero cross stiffness of the honeycomb, this fraction will always be 0.5 for a symmetrical

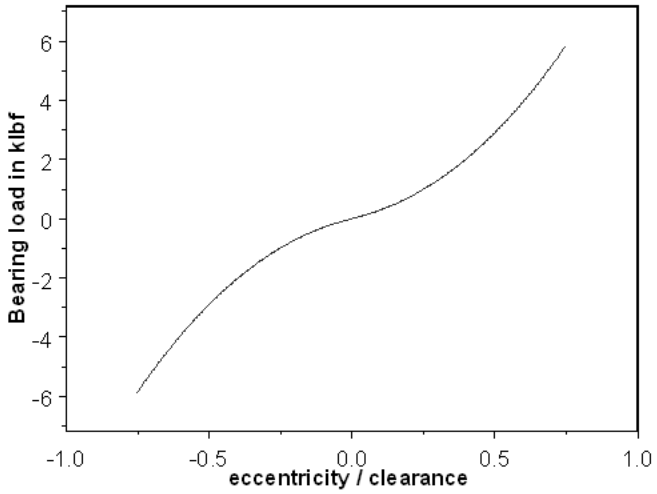

Figure 27. Radial Bearing Load Model Used to Calculate Static Equilibrium of Rotor.

between-bearings rotor, as can be seen near the center of the plot, where the direct and cross stiffnesses equal zero.) The loads are expressed as radial values to make a simple plot. Note the direction of the load can completely reverse as the stiffness changes, but this is hidden in Figures 28 and 29. This calculation shows a remarkable peak in the bearing load at about negative 4 million pounds per inch direct stiffness and at zero cross-coupled stiffness. The calculated radial load changes abruptly, and some mathematical technique was required to make this plot.

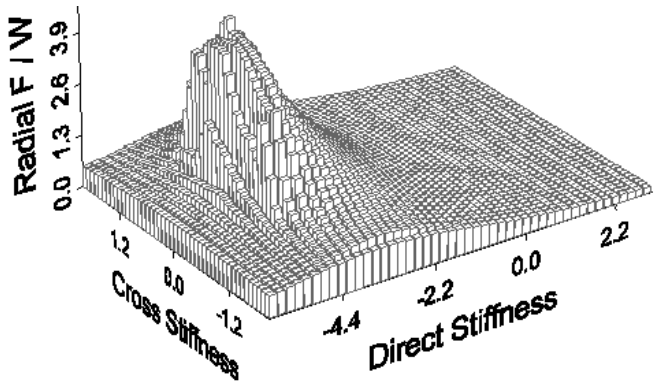

Figure 28. Radial Bearing Force Normalized by Rotor Weight, for Bearing Nearer to Honeycomb Balance Piston. (Honeycomb stiffness is in millions of lbf/in.)

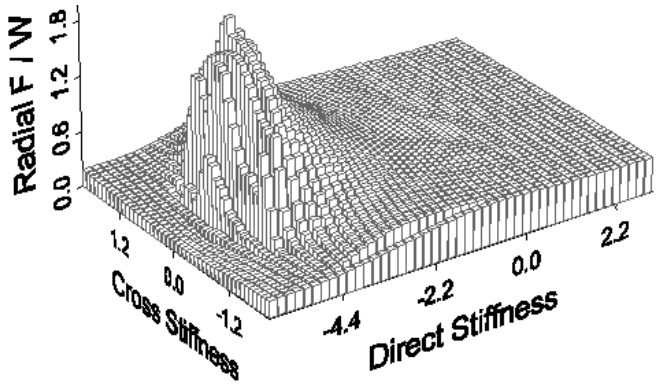

Figure 29. Radial Bearing Force Normalized by Rotor Weight, for Bearing Farther from Honeycomb Balance Piston. (Honeycomb stiffness is in millions of lbf/in.)

Figures 28 and 29 show that direct negative stiffness can produce strong changes in rotor static equilibrium. These in turn will affect the synchronous response of even less flexible rotors. Positive direct stiffness will produce weaker changes, mainly reducing bearing load somewhat. To be complete would require calculation of the bearing loads at the beginning of the rotordynamics analysis, for the expected honeycomb distortions. In practice it is better to avoid tight clearance and diverging clearance in the direction of flow for honeycomb seals.

CONCLUSIONS

- The honeycomb seal has the capability to control rotor stability.
- The honeycomb seal can produce strong negative stiffness (effective value) if the clearance is divergent in the direction of flow.
- Given inlet swirl (no shunt) the honeycomb seal can produce strong cross-coupled stiffness (effective value), which can cause rotor instability.
- The honeycomb is very sensitive to operating clearance.

Nishida and Kobayashi's (Kobayashi, et al., 1990) criteria for rotating stall in a vaneless diffuser is verified within one degree (gas angle error) provided an appropriate pinch schedule is used.

APPENDIX

The linearized model for force acting on the rotor is defined by Childs (1993) as follows for circular centered orbits:

$$\begin{pmatrix} Fx \\ Fy \end{pmatrix} = -1 \times \left[\begin{pmatrix} K & k \\ -k & K \end{pmatrix} \times \begin{pmatrix} X \\ Y \end{pmatrix} + \begin{pmatrix} C & c \\ -c & C \end{pmatrix} \times \begin{pmatrix} Xdot \\ Ydot \end{pmatrix} \right] \quad \text{(A-1)}$$

where:

C,c	=	Direct and cross-coupled damping coefficients (F*T/L)
Fx	=	Force in X direction acting on the rotor (F)
Fy	=	Force in Y direction acting on the rotor (F)
K, k	=	Direct and cross-coupled stiffness coefficients (F/L)
X, Y	=	Displacements with respect to Cartesian coordinates in an inertial reference frame (L)
Xdot, Ydot	=	Time derivatives of the displacements (L/T)

Based on the above model, the effective stiffness, K_{eff}, and the effective damping, C_{eff}, are defined as follows:

$$Keff = K - c \cdot whirl \quad \text{(A-2)}$$

where:
whirl = Frequency of the circular orbit

$$Ceff = C - \frac{k}{whirl} \quad \text{(A-3)}$$

Note that these effective values are *not constant with whirl frequency*, and therefore the damped natural frequency calculation for log dec must be iterated on whirl frequency.

REFERENCES

API Standard 617, 2002, "Axial and Centrifugal Compressors and Expander-Compressors for Petroleum, Chemical and Gas Industry Services," Seventh Edition, American Petroleum Institute, Washington, D.C.

ASME PTC-10, 1997, "Performance Test Code on Compressors and Exhausters," American Society of Mechanical Engineers, New York, New York.

Childs, D. W., 1993, *Turbomachinery Rotordynamics: Phenomena, Modeling, and Analysis*, New York, New York: John Wiley & Sons, Inc.

Fulton, J. W, 1984a, March 1984, "The Decision to Full Load Test a High Pressure Centrifugal Compressor in its Module Prior to Tow-Out," IMechE Second European Congress, *Fluid Machinery for the Oil, Petrochemical and Related Industries*, The Hague, The Netherlands.

Fulton, J. W., 1984b, "Full Load Testing in the Platform Module Prior to Tow Out: A Case History of Subsynchronous Instability," Rotordynamic Instability Problems in High PerformanceTurbomachinery, NASA Conference Publication 2338, Texas A&M University, College Station, Texas, pp. 1-16.

Fulton, J. W. and Blair, W. G, 1995, "Experience with Empirical Criteria for Rotating Stall in Radial Vaneless Diffusers," Turbomachinery Laboratory, Texas A&M University, College Station, Texas, pp. 97-106.

Kleynhans, G. W. and Childs, D. W, 1997, "The Acoustic Influence of Cell Depth on Rotordynamic Characteristics of Smooth-Rotor/Honeycomb-Stator Annular Gas Seals," *Journal of Engineering for Gas Turbines and Power*, *119*, pp. 949-957.

Kobayashi, H., Nishida, H., Takaya, T., and Fukushima, Y., September 1990, "A Study on the Rotating Stall of Centrifugal Compressors," Second Report, Effect of Vaneless Diffuser Inlet Shape on Rotating Stall, pp. 98-103.

Murphy, B. T., 1993, "RAPP & PUP USER MANUAL," Rotordynamics-Seal Research, Inc., Simi Valley, California.

Nicholas, J. C., Gunter, E. J., and Allaire, P.E., April 1979, "Stiffness and Damping Coefficients for the Five Pad Tilting Pad Bearing," ASLE Transactions, *22*, (2), pp. 112-124.

ACKNOWLEDGEMENTS

The authors recognize GE Oil & Gas Nuovo Pignone, ExxonMobil Research & Engineering Company, and ExxonMobil Development Company for permission to publish the paper. Also gratitude is given to all who contributed, with special thanks to Dr. Leonardo Baldassarre and Mr. Enrico Leone of GE Oil & Gas Nuovo Pignone, and Mr. Vincent Mankowski and Mr. George Hayles of ExxonMobil Research & Engineering Company for their support and efforts during the testing and analysis.